Evidence for a Mechanism by Which ω-3 Polyunsaturated Lipids May Affect Membrane Protein Function†

Mauricio Carrillo-Tripp and Scott E. Feller*

Department of Chemistry, Wabash College, 301 West Wabash Avenue, Crawfordsville, Indiana 47933

Received May 4, 2005; Revised Manuscript Received June 7, 2005

ABSTRACT: We have calculated the lateral pressure profile from well-converged, experimentally validated, molecular dynamics simulations of hydrated lipid bilayer membranes containing highly polyunsaturated fatty acids. The three simulations, each 30 ns in length, contain ω-3 fatty acids, ω-6 fatty acids, and a mixture of ω-3 fatty acids and cholesterol and were continued from previously published simulations that demonstrated excellent agreement with a wide variety of experimental measurements. We find that the distribution of lateral stress within the hydrophobic core of the membrane is sensitively dependent on the degree of chain unsaturation and on the presence of cholesterol. Replacing ω-3 fatty acids with ω-6 chains, or incorporating cholesterol into the membrane, shifts the repulsive lateral chain pressure away from the lipid/water interface toward the bilayer interior. This may support a previously proposed mechanism by which lipid composition may affect conformational equilibrium for integral membrane proteins.

The literature describing the effects of polyunsaturated fatty acids (PUFA), on systems ranging from model membranes to whole organisms, is vast; e.g., see ref *1* and references cited therein. A range of pathologies are associated with insufficient dietary levels of PUFA, particularly the class referred to as ω-3 fatty acids. Docosahexaenoic acid (DHA, 22:6n3), the most prevalent of the ω-3 acids, consists of a 22 carbon chain with 6 double bonds and is found in high concentrations (up to 50 mol %) in the receptor-rich cell membranes of the central nervous system. Insufficient levels of DHA in the diet, especially in the developing infant, lead to decreased mental function and visual acuity (*2*, *3*). A broader role for DHA is suggested by the observation that changes in the lower levels (<5%) at which it is found in cells outside the nervous system also have significant biological effects; for example, DHA levels are associated with pathologies as diverse as rheumatoid arthritis, cystic fibrosis, and alcoholism (*4*−*6*). The unique role of DHA is powerfully demonstrated by observations, from experiments probing both the molecular level and the whole organism, that replacement of DHA by docosapentaenoic acid (DPA, 22:5n6), a fatty acid of identical length but with one double bond removed, leads to significant changes. For example, Gawrisch and co-workers showed, from nuclear magnetic resonance (NMR) and X-ray scattering experiments on model membranes, that the structure and dynamics of lipid bilayers containing DHA and DPA are quite different, most notably in the acyl chain dynamics and in the distribution of acyl chain densities along the membrane normal (*7*). Litman and co-workers showed that in retinal rod outer segment membranes isolated from rats fed with a ω-3 deficient diet, DHA had been replaced by DPA and that this replacement correlated with reduced rhodopsin activation and slower formation of metarhodopsin II (*8*). In rats, Moriguchi and Salem observed losses in brain function associated with DHA-deficient diets that could be partially reversed with a DHA-supplemented diet (*9*).

How could a single molecular species influence such a diverse array of biological processes? And how could such a minor change in molecular structure as the transformation of a single cis unsaturation to methylene groups have such dramatic effects? Stillwell and Wassall, in a recent review, argued that the accumulated evidence suggests that the mechanism is physical, as opposed to biochemical, and is based on the role of the fatty acids in lipid bilayers as the solvent environment for membrane proteins (*1*). We have previously used atomic-level molecular dynamics (MD) computer simulation techniques to identify specific attractive interactions between DHA and rhodopsin (*10*), a membrane protein from the family of G protein coupled receptors (GPCR). In addition to this type of short-range effect, essentially the formation of a laterally heterogeneous microdomain by the protein species, there may be other, less direct, mechanisms by which DHA content may influence membrane protein stability (*11*−*14*). In the following, we examine one such mechanism, the lateral pressure profile (LPP) theory developed by Cantor. Using detailed computer simulations, providing extremely high spatial resolution, we have computed the LPP from trajectories of DHA- and DPA-containing lipids. These simulations follow the protocols used in our previous work, where we validated simulation methodologies and empirical energy parameters via close comparison with experimental data on these lipids (*7*, *15*, *16*). Additionally, we have examined the effect of cholesterol on the LPP in a DHA-containing membrane, due partly to the ubiquity of cholesterol in plasma membranes but more

† This work was supported by the National Science Foundation through Award MCB-0091508.

* Address correspondence to to this author. E-mail: fellers@wabash.edu. Phone: (765) 361-6175. Fax: (765) 361-6149.

10.1021/bi050822e CCC: $30.25
Published on Web 07/06/2005

specifically to address potentially unique interactions between cholesterol and polyunsaturated lipids (*15*, *17*).

THEORY

We review here briefly the theoretical work of Cantor; for a more detailed account the reader is referred to refs *12*−*14*. The central concept of the LPP is that the forces acting in the plane of the membrane bilayer (lateral pressures) are a function of the position along the bilayer normal, i.e., $P_L = P_L(z)$, where z is the coordinate describing the position along the membrane normal (in this work we will take $z = 0$ as the center of the hydrophobic core of the bilayer), while the component of the pressure parallel to the bilayer normal (P_N) will be uniform throughout the bilayer. The lateral pressure is an inherently microscopic property; thus there is no direct experimental probe of this function. It can be shown, however, that various integral moments of the LPP can be related to macroscopic quantities; for example, the integral of $P_N - P_L(z)$ over all z gives the surface tension while bending elastic properties are functions of the first and second integral moments, respectively (*18*). As described in ref *19*, the LPP will determine protein conformational equilibria in the case where the conformational states of the protein, e.g., R ↔ P, have different cross-sectional areas (A), i.e., $A_R(z) \neq A_P(z)$ for some values of z. The free energy of each conformational state will be influenced by the amount of work done against the force of the lateral pressure arising from the lipid bilayer:

$$w = -\int P_L(z)\Delta A(z)\, dz \quad (1)$$

The stabilization or destabilization of one state as compared to another will thus depend on details of the protein shape through its cross-sectional area profile and the values of the lateral pressure acting on all regions where a change in cross-sectional area occurs. If changes in lipid composition alter the LPP, the equilibrium constant for the protein conformational states will change by an amount $e^{-\alpha}$ where

$$\alpha = \frac{1}{kT}\int \Delta P_L(z)\Delta A(z)\, dz \quad (2)$$

where k is the Boltzmann constant and T is the absolute temperature. Thus the differences in pressure profiles (between lipids) and cross-sectional areas (between protein conformations) are key to calculating the effect of membrane composition on protein conformation. The LPP has in the past been computed from bilayer models with varying complexity, including mean-field lattice models of acyl chains (*13*), dissipative particle dynamics of coarse-grained amphiphiles (*20*, *21*), and more recently from atomic-level MD simulations of phospholipid bilayers (*22*−*24*).

METHODS

The starting point of each simulation was the final frame (approximately 20 ns point) of previously published simulations of the three systems: a hydrated 1-stearoyl-2-docosahexaenoyl-*sn*-glycero-3-phosphocholine (18:0-22:6n3PC) bilayer (*16*), a hydrated 1-stearoyl-2-docosapentaenoyl-*sn*-glycero-3-phosphocholine (18:0-22:5n6PC) bilayer (*7*), and a mixed bilayer of 18:0-22:6n3PC containing 25 mol % cholesterol (*15*). A description of the simulation methodology, details of the observed structural and dynamic properties, and comparisons with experimental data can be found in refs *7*, *15*, and *16*. Each system contained 72 lipid molecules in full atomic detail; the pure lipid systems contained 15.1 water molecules per lipid while the cholesterol-containing system had an additional 24 cholesterol molecules and 30.2 waters per lipid. All simulations were carried out using the parallel molecular dynamics program NAMD (*25*) with the CHARMM22 all-atom empirical potential energy parameters for lipids (*26*, *27*) and its extension to polyunsaturated lipids (*16*). A cutoff of 10 Å was employed for the Lennard-Jones interactions (switched smoothly to zero over a 1 Å interval) and the real space portion of the particle mesh Ewald method (*28*). An FFT grid density of ~1/Å was used. All covalent bonds involving hydrogen were fixed at their equilibrium distances using the SHAKE algorithm (*29*). A partially flexible simulation cell was employed with the z dimension (i.e., the bilayer normal) adjusted to maintain a constant pressure of 1 atm using the Langevin piston method (*30*), and the x and y dimensions were fixed to maintain a constant area per molecule in the plane of the membrane. Periodic boundary conditions in all three dimensions were used to eliminate edge effects. Velocities were reassigned every 1 ps to maintain a constant temperature of 303 K. A time step of 2 fs was used in all simulations. Total simulation length was 30 ns in each case. A surface tension of ~10 dyn/cm was observed in each simulation, consistent with earlier results using this force field and this number of lipids.

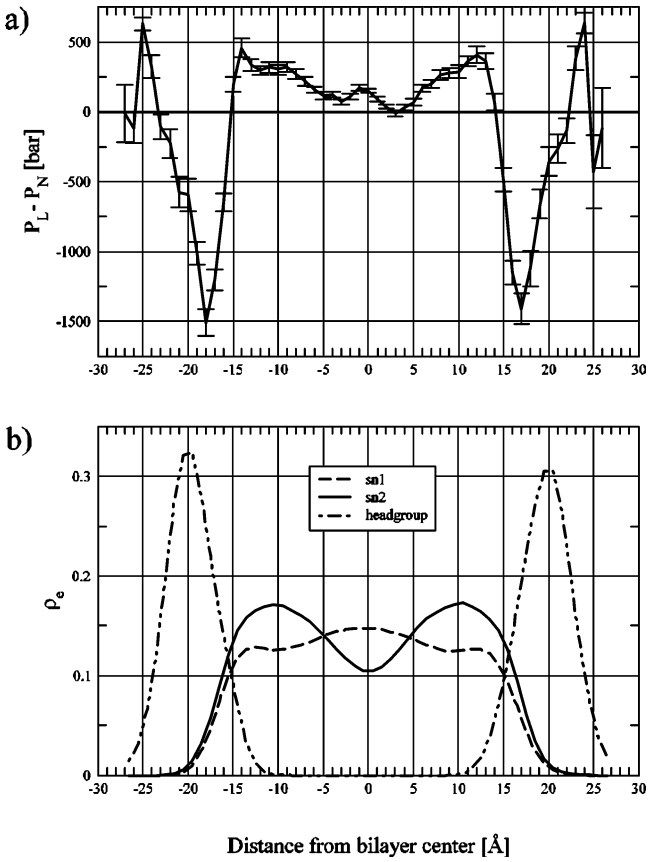

FIGURE 1: Analysis for 18:0-22:6n3PC. (a) Difference between lateral pressure (P_L) and normal pressure (P_N) as a function of transverse position. Error bars represent the standard error in the mean, SE = $\sigma/(N)^{1/2}$, where the standard deviation was calculated from N averages of 1 ns simulation blocks. (b) Density profiles for the three components of the lipid.

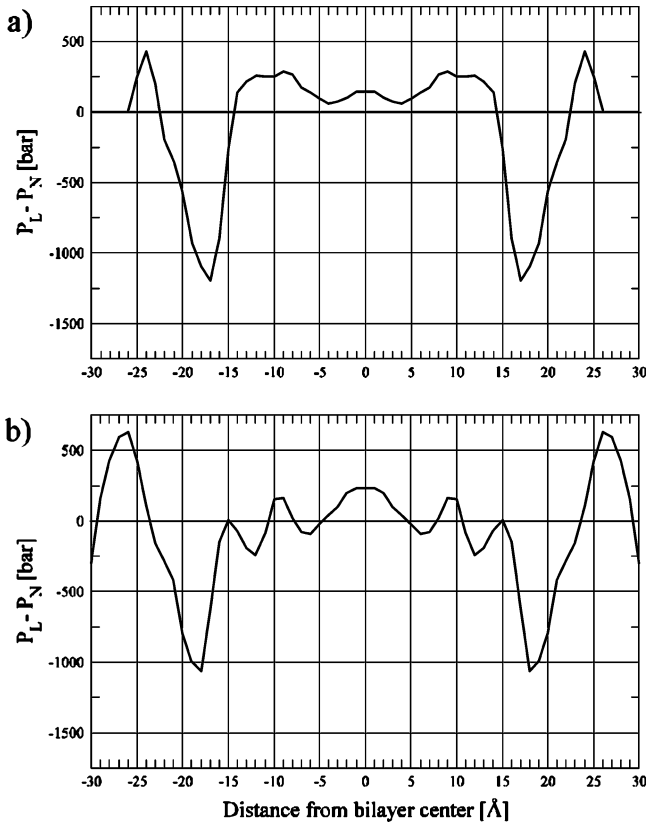

FIGURE 2: Lateral pressure profile for (a) 18:0-22:5n6PC and (b) a mixture of 18:0-22:6n3PC and cholesterol. The time averaged results are further averaged over the two equivalent monolayers, resulting in symmetrized results.

The lateral pressure was calculated as described in refs *23* and *24*. Care was taken to remove small translations in the bilayer center of mass, arising from numerical imprecision, to maintain a constant spatial location throughout the simulation. Contributions from the kinetic and bonded potential contributions to the pressure were computed at each time step during the simulation. Contributions from nonbonded interactions (i.e., Lennard-Jones and electrostatic terms) were postprocessed from coordinate frames saved every 1 ps in the molecular dynamics trajectory with the force truncated at a distance of 20 Å. The simulation cell was sliced along the *z* dimension using bins perpendicular to the bilayer normal ≈1 Å thick. The LPP was computed and averaged over the full 30 ns for each bin. Simulations were carried out with sixteen 2.4 GHz processors of a Beowulf-type parallel computer, with each nanosecond of simulation taking approximately 8 h of wall time. Values of the pressure profile will depend somewhat on technical details of the calculation, such as the choice of truncation length for the van der Waals interactions and the way in which forces are distributed among slabs (see refs *22*−*24* and *31*); thus we focus in this report on differences in the pressure profile which are largely independent of algorithm. A recent report describing a very careful analysis of the pressure profile in a fluid phase phosphatidylcholine bilayer showed that the approach used here, i.e., evaluating the pressure profile with a large cutoff distance from a trajectory generated using Ewald summation, gave quite reliable pressure profiles provided a cutoff of at least 16 Å was employed for the analysis (*31*).

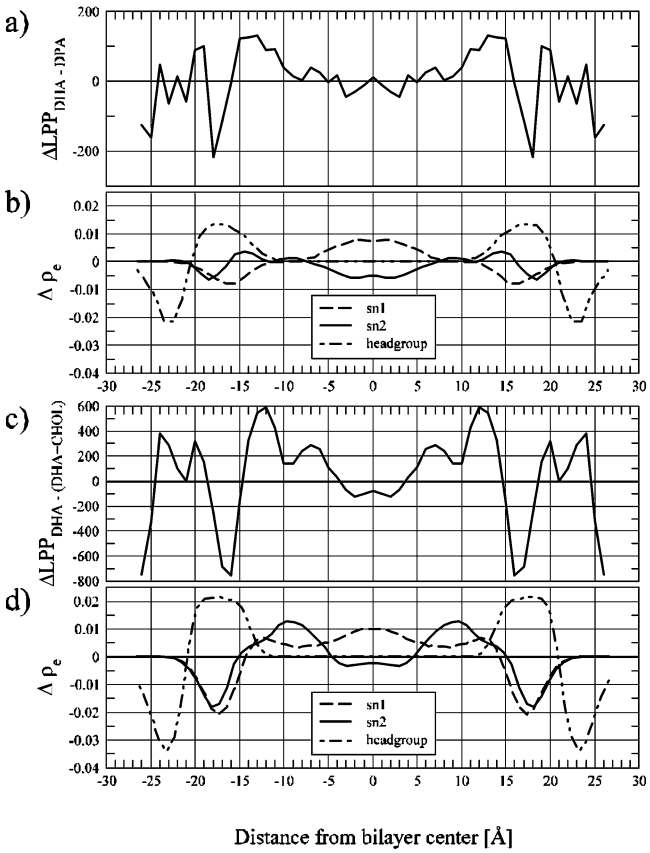

FIGURE 3: Differences in lateral pressure profiles (a and c) and component densities (b and d) when comparing 18:0-22:6n3PC with 18:0-22:5n6PC (a and b) and with a mixture of 18:0-22:6n3PC and cholesterol (c and d). Statistically significant ($p < 0.05$) differences between 18:0-22:6n3PC and 18:0-22:5n6PC (a) are observed in the upper acyl chain region (10 Å < $|z|$ < 15 Å). Statistically significant differences are observed upon cholesterol incorporation (c) for the entire bilayer interior ($|z|$ < 20 Å).

RESULTS

Figure 1a shows the lateral pressure profile calculated from the simulation of the 18:0-22:6n3PC bilayer. The magnitudes of the lateral pressures may seem surprisingly large; however, their magnitude had been predicted previously on the basis of estimates from interfacial tensions and the thickness of the lipid/water interface (*32*). Uncertainties in the pressure function were calculated from 1 ns block averages (*33*) based on an analysis of autocorrelation functions for various *z* positions that showed correlation times ranged from tens to hundreds of picoseconds. Notably, the most precisely determined region of the LPP is the hydrophobic core of the membrane that is the focus of the present study. The results are qualitatively similar to those reported from other MD simulations (*22*, *23*), with a positive contribution from the hydrophobic core ($|z|$ < 15 Å) and the lipid headgroup/water interface (23 Å < $|z|$ < 26 Å) largely balanced by negative contributions arising from the interfacial tension at the hydrophobic/hydrophilic surface. (Figure 1b shows the location of the various interfaces.) More quantitatively, the integrated pressures in these regions correspond approximately to contributions of −11, +55, and −30 dyn/cm to the surface tension. The LPP does not reach zero in the water layer because the simulation conditions correspond to a water concentration slightly below full hydration. Test simulations at higher hydration showed that the LPP reaches zero with

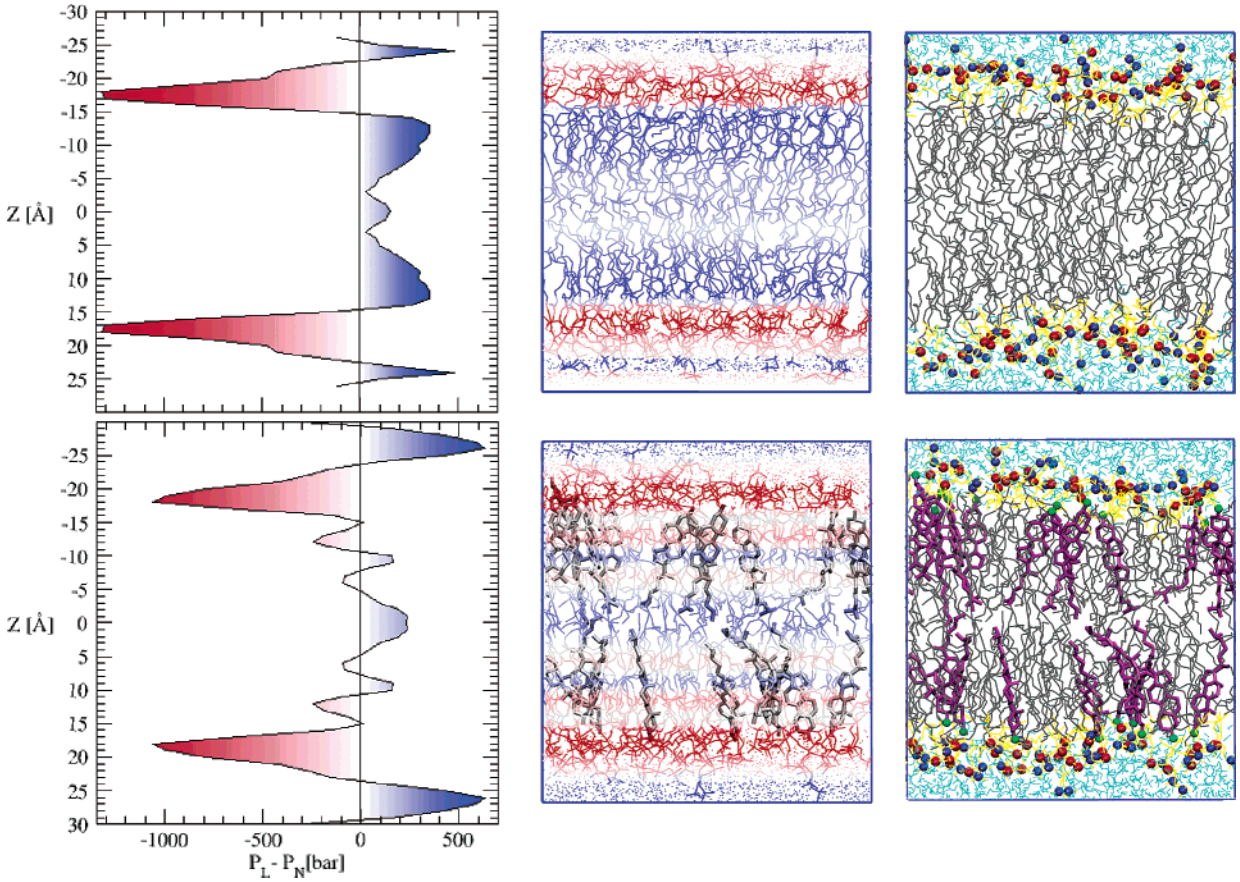

FIGURE 4: Graphical representations of the lateral pressure profile. On the left are the lateral pressure profiles for 18:0-22:6n3PC (top) and 18:0-22:6n3PC + cholesterol (bottom), color coded by the magnitude and sign of the lateral pressure. In the center are molecular graphics of a snapshot of the simulation with atoms colored on the basis of the local lateral pressure. On the right is a second representation of the same configuration that emphasizes the location of the lipid headgroups and sterol rings.

a unit cell that is approximately 6 Å greater in z with no statistically significant effect on the bilayer interior.

Upon close inspection, significant differences are seen in the distribution of chain pressure when the present polyunsaturated lipid is compared with previous reports on saturated (*22*) and monounsaturated (*23*, *24*) phosphatidylcholines. The magnitude of the chain pressure near the interface ($|z| \approx 15$ Å) is much larger in the DHA-containing lipid; e.g., the chain pressure at the center of the bilayer is greater than or comparable to the chain pressure at the interface in the saturated and monounsaturated systems, while the polyunsaturated system shows a much greater pressure at the top of the acyl chains than anywhere else within the hydrophobic core. It should be noted that this trend was also predicted by the mean-field lattice model calculations of Cantor (*13*). The agreement between the atomic-level MD models, that had previously been validated through comparison with experimental measurements probing molecular level DHA structure (*7*, *16*), and the mean-field calculations, that had successfully reproduced a number of macroscopic material properties of the membrane (*13*), provides strong evidence for the view that an effect of polyunsaturation is to shift the chain pressure from the bilayer interior to the interface.

Figure 2a gives the LPP for 18:0-22:5n6PC. The magnitude of both the positive chain pressure and the negative pressure at the interface are decreased in this DPA-containing lipid, such that the integrated lateral pressure is very nearly the same in 22:6 and 22:5, in accord with the experimental observation that their molecular surface areas are identical within experimental error (*7*). To allow a more quantitative analysis, we have calculated the difference in the lateral pressure profiles of 18:0-22:6n3PC and 18:0-22:5n6PC and plotted the result in Figure 3a, along with the difference in lipid density profiles that is presented as Figure 3b. Differences are small across much of the bilayer; however, statistically significant differences in the LPP ($p < 0.05$) between 18:0-22:6n3PC and 18:0-22:5n6PC are observed in the upper acyl chain region (10 Å $< |z| <$ 15 Å). Comparing changes in the pressure profile with changes in the chain density is quite illuminating, allowing the connection to be made between small changes in molecular structure and the shifts in lateral pressure distribution. Replacement of DHA by DPA results in a shift of polyunsaturated acyl chain density from the interfacial region to the bilayer center, accompanied by a complementary change in the stearic acid distribution. Analysis of the pressure profile data indicates that this shift, observed in our previous simulations and verified experimentally (*7*), is accompanied by a statistically significant decrease in chain pressure at the interface. In other words, the repulsive chain pressure follows the distribution of polyunsaturated acyl chain segments, as is clearly seen by comparing ΔP in Figure 3a with $\Delta\rho_e(sn2)$ in Figure 3b.

The effect of cholesterol addition is shown in Figures 2b and 3c,d. The shifts in lateral pressure are much more dramatic than the case of acyl chain substitution described above (statistically significant differences are observed for essentially the entire bilayer interior, $|z| <$ 20 Å); however, the analysis is complicated somewhat by the change in

bilayer thickness accompanying cholesterol incorporation. The same general trend is observed, however, in that a shift in polyunsaturated chain density from the interface to the center of the bilayer is correlated with the migration of lateral stress. Essentially, the effect of cholesterol addition is to produce an LPP that more closely resembles a saturated or monounsaturated system. One feature unique to the LPP of the cholesterol-containing system is the existence of additional local maxima and minima in the pressure through the hydrocarbon core. We have been unable to ascribe this nonmonotonic behavior to structural details of the lipid or sterol, though it may be related to the general ordering effect of cholesterol. That the addition of 25 mol % cholesterol could fundamentally alter the LPP suggests that cholesterol concentration is a variable that could sensitively tune conformational equilibria for membrane proteins that undergo a change in cross-sectional area, especially a change that occurred in the upper acyl chain region or near the membrane center (where especially large pressure redistributions are observed).

CONCLUSIONS

We have provided quantitative values of the lateral pressure profile within a bilayer membrane and demonstrated that small changes in molecular structure, e.g., ω-3 vs ω-6 fatty acids or incorporation of cholesterol, can lead to shifts in the local pressure on the order of hundreds of bars. If these pressure shifts are correlated with changes in the cross-sectional area distribution of a membrane protein, conformational equilibrium will be shifted (eq 2). Calculations suggest that, with the pressure shifts described here, only modest changes in cross-sectional area would result in dramatic shifts in conformational equilibria (*19*). Unfortunately, atomic-level structures of membrane proteins are notoriously difficult to obtain, and there are currently no cases of crystallographic structures for a transmembrane protein differing only in its conformational state. An excellent candidate for such a study is rhodopsin, an integral membrane protein for which a ground (dark-adapted) structure is known (*34*). Furthermore, both replacement of DHA by DPA and the incorporation of cholesterol have been observed to affect conformational equilibria critical to the rhodopsin photocycle (*35*). Interestingly, both of these effects act to slow the photocycle, as the present simulations would predict if activation involved a decrease in protein cross-sectional area in the upper acyl chain region. Recent experimental work (*36*) on rhodopsin indicates that absorption of light leads to an elongation of the protein, presumably involving a decrease in the cross-sectional area in at least certain regions of the protein. The magnitude and location of the area shift is unknown; however, a recent MD simulation calculation of the cross-sectional area profile of rhodopsin (*37*) shows that it is highly nonuniform (fluctuations of 20% from the mean), suggesting that details of helix orientation and packing could lead to substantial changes in the local cross-sectional area. Additionally, the protein cross-sectional area is greatest in the lipid upper acyl chain region. A more quantitative determination of the cross-sectional area profile of the activated state would allow a rigorous test of the pressure redistributions predicted by these simulations.

ACKNOWLEDGMENT

We thank J. Gullingsrud for help with technical details of the pressure profile calculation.

REFERENCES

1. Stillwell, W., and Wassall, S. R. (2003) Docosahexaenoic acid: membrane properties of a unique fatty acid, *Chem. Phys. Lipids 126*, 1−27.
2. Menkes, J. H., Alter, M., Steigleder, G. K., Weakley, D. R., and Sung, J. H. (1962) A sex-linked recessive disorder with retardation of growth, peculiar hair, and focal cerebral and cerebellar degeneration, *Pediatrics 29*, 764−779.
3. Birch, E. E., Birch, D. G., Hoffman, D. R., and Uauy, R. (1992) Dietary essential fatty acid supply and visual acuity development, *Invest. Ophthalmol. Visual Sci. 33*, 3242−3253.
4. Kremer, J. M., Lawrence, D. A., Jubiz, W., DiGiacomo, R., Rynes, R., Bartholomew, L. E., and Sherman, M. (1990) Dietary fish oil and olive oil supplementation in patients with rheumatoid arthritis. Clinical and immunologic effects, *Arthritis Rheum. 33*, 810−820.
5. Freedman, S. D., Katz, M. H., Parker, E. M., Laposata, M., Urman, M. Y., and Alvarez, J. G. (1999) A membrane lipid imbalance plays a role in the phenotypic expression of cystic fibrosis in cftr(−/−) mice, *Proc. Natl. Acad. Sci. U.S.A. 96*, 13995−14000.
6. Pawlosky, R. J., and Salem, N., Jr. (1995) Ethanol exposure causes a decrease in docosahexaenoic acid and an increase in docosapentaenoic acid in feline brains and retinas, *Am. J. Clin. Nutr. 61*, 1284−1289.
7. Eldho, N. V., Feller, S. E., Tristram-Nagle, S., Polozov, I. V., and Gawrisch, K. (2003) Polyunsaturated docosahexaenoic vs docosapentaenoic acid-differences in lipid matrix properties from the loss of one double bond, *J. Am. Chem. Soc. 125*, 6409−6421.
8. Niu, S. L., Mitchell, D. C., Lim, S. Y., Wen, Z. M., Kim, H. Y., Salem, N., Jr., and Litman, B. J. (2004) Reduced G protein-coupled signaling efficiency in retinal rod outer segments in response to n-3 fatty acid deficiency, *J. Biol. Chem. 279*, 31098−31104.
9. Moriguchi, T., and Salem, N., Jr. (2003) Recovery of brain docosahexaenoate leads to recovery of spatial task performance, *J. Neurochem. 87*, 297−309.
10. Feller, S. E., Gawrisch, K., and Woolf, T. B. (2003) Rhodopsin exhibits a preference for solvation by polyunsaturated docosahexaenoic acid, *J. Am. Chem. Soc. 125*, 4434−4435.
11. Botelho, A. V., Gibson, N. J., Thurmond, R. L., Wang, Y., and Brown, M. F. (2002) Conformational energetics of rhodopsin modulated by nonlamellar-forming lipids, *Biochemistry 41*, 6354−6368.
12. Cantor, R. S. (2002) Size distribution of barrel-stave aggregates of membrane peptides: influence of the bilayer lateral pressure profile, *Biophys. J. 82*, 2520−2525.
13. Cantor, R. S. (1999) Lipid composition and the lateral pressure profile in bilayers, *Biophys. J. 76*, 2625−2639.
14. Cantor, R. S. (1998) The lateral pressure profile in membranes: a physical mechanism of general anesthesia, *Toxicol. Lett. 100−101*, 451−458.
15. Pitman, M. C., Suits, F., Mackerell, A. D., Jr., and Feller, S. E. (2004) Molecular-level organization of saturated and polyunsaturated fatty acids in a phosphatidylcholine bilayer containing cholesterol, *Biochemistry 43*, 15318−15328.
16. Feller, S. E., Gawrisch, K., and MacKerell, A. D., Jr. (2002) Polyunsaturated fatty acids in lipid bilayers: intrinsic and environmental contributions to their unique physical properties, *J. Am. Chem. Soc. 124*, 318−326.
17. Polozova, A., and Litman, B. J. (2000) Cholesterol dependent recruitment of di22:6-PC by a G protein-coupled receptor into lateral domains, *Biophys. J. 79*, 2632−2643.
18. Szleifer, I., Kramer, D., Ben-Shaul, A., Gelbart, W. M., and Safran, S. A. (1990) Molecular theory of curvature elasticity in surfactant films, *J. Chem. Phys. 92*, 6800−6817.
19. Cantor, R. S. (1997) Lateral pressures in cell membranes: a mechanism for modulation of protein function, *J. Phys. Chem. B 101*, 1723−1725.
20. Shillcock, J. C., and Lipowsky, R. (2002) Equilibrium structure and lateral stress distribution of amphiphilic bilayers from dissipative particle dynamics simulations, *J. Chem. Phys. 117*, 5048−5061.

21. Venturoli, M., and Smit, B. (1999) Simulating the self-assembly of model membranes, *Phys. Chem. Commun. 10*, 1−5.
22. Lindahl, E., and Edholm, O. (2000) Spatial and energetic-entropic decomposition of surface tension in lipid bilayers from molecular dynamics simulations, *J. Chem. Phys. 113*, 3882−3893.
23. Gullingsrud, J., and Schulten, K. (2004) Lipid bilayer pressure profiles and mechanosensitive channel gating, *Biophys. J. 86*, 3496−3509.
24. Gullingsrud, J., and Schulten, K. (2003) Gating of MscL studied by steered molecular dynamics, *Biophys. J. 85*, 2087−2099.
25. Kale, L., Skeel, R., Bhandarkar, M., Brunner, R., Gursoy, A., Krawetz, N., Phillips, J., Shinozaki, A., Varadarajan, K., and Schulten, K. (1999) NAMD2: greater scalability for parallel molecular dynamics, *J. Comput. Phys. 151*, 283−312.
26. Schlenkrich, M., Brickmann, J., MacKerell, A. D., Jr., and Karplus, M. (1996) Empirical potential energy function for phospholipids: criteria for parameter optimization and applications, in *Biological Membranes: A Molecular Perspective from Computation and Experiment* (Merz, K., and Roux, B., Eds.) pp 31−81, Birkhauser, Boston, MA.
27. Feller, S. E., and MacKerell, A. D., Jr. (2000) An improved empirical potential energy function for molecular simulations of phospholipids, *J. Phys. Chem. B 104*, 7510−7515.
28. Essmann, U., Perera, L., Berkowitz, M. L., Darden, T., Lee, H., and Pedersen, L. G. (1995) A smooth particle mesh Ewald method, *J. Chem. Phys. 103*, 8577.
29. Ryckaert, J. P., Ciccotti, G., and Berendsen, H. J. C. (1977) Numerical integration of the Cartesian equations of motion of a system with constraints: molecular dynamics of *n*-alkanes, *J. Comput. Phys. 23*, 327−341.
30. Feller, S. E., Zhang, Y., Pastor, R. W., and Brooks, B. R. (1995) Constant pressure molecular dynamics simulation: The Langevin piston method, *J. Comput. Phys. 103*, 4613.
31. Sonne, J., Hansen, F. Y., and Gunther, P. H. (2005) Methodological problems in pressure profile calculations for lipid bilayers, *J. Chem. Phys. 122*, 124903−124911.
32. Cantor, R. S. (1997) The lateral pressure profile in membranes: a physical mechanism of general anesthesia, *Biochemistry 36*, 2339−2344.
33. Allen, M. P., and T., D. J. (1987) *Computer Simulation of Liquids*, Clarendon, Oxford.
34. Palczewski, K., Kumasaka, T., Hori, T., Behnke, C. A., Motoshima, H., Fox, B. A., Le Trong, I., Teller, D. C., Okada, T., Stenkamp, R. E., Yamamoto, M., and Miyano, M. (2000) Crystal structure of rhodopsin: A G protein-coupled receptor, *Science 289*, 739−745.
35. Niu, S. L., Mitchell, D. C., and Litman, B. J. (2001) Optimization of receptor-G protein coupling by bilayer lipid composition II: formation of metarhodopsin II-transducin complex, *J. Biol. Chem. 276*, 42807−42811.
36. Alves, I. D., Salgado, G. F., Salamon, Z., Brown, M. F., Tollin, G., and Hruby, V. J. (2005) Phosphatidylethanolamine enhances rhodopsin photoactivation and transducin binding in a solid supported lipid bilayer as determined using plasmon-waveguide resonance spectroscopy, *Biophys. J. 88*, 198−210.
37. Pitman, M. C., Grossfield, A., Suits, F., and Feller, S. E. (2005) Role of cholesterol and polyunsaturated chains in lipid−protein interactions: molecular dynamics simulation of rhodopsin in a realistic membrane environment, *J. Am. Chem. Soc. 127*, 4576−4577.

BI050822E